Published in final edited form as:

Nat Chem Biol. 2020 April ; 16(4): 400–407. doi:10.1038/s41589-020-0499-8.

Crystal structure of human PLD1 provides insight into activation by PI(4,5)P_2 and RhoA

Forrest Z. Bowling[1], **Christian M. Salazar**[2], **Justin A. Bell**[1], **Tahrima S. Huq**[1], **Michael A. Frohman**[2], **Michael V. Airola**[1,*]

[1]Department of Biochemistry and Cell Biology, Stony Brook University, Stony Brook, New York

[2]Department of Pharmacological Sciences, Stony Brook University, Stony Brook, New York

Abstract

The signal transduction enzyme phospholipase D1 (PLD1) hydrolyzes phosphatidylcholine to generate the lipid second-messenger phosphatidic acid, which plays roles in disease processes such as thrombosis and cancer. PLD1 is directly and synergistically regulated by Protein Kinase C, Arf and Rho GTPases, and the membrane lipid phosphatidylinositol-4,5-bisphosphate (PIP_2). Here, we present a 1.8Å-resolution crystal structure of the human PLD1 catalytic domain that is characterized by a globular fold with a funnel-shaped hydrophobic cavity leading to the active site. Adjacent is a PIP_2-binding polybasic pocket at the membrane interface that is essential for activity. The C-terminus folds into and contributes part of the catalytic pocket, which harbors a phosphohistidine that mimics an intermediate stage of the catalytic cycle. Mapping of PLD1 mutations that disrupt RhoA activation identifies the RhoA-PLD1 binding interface. This structure sheds light on PLD1 regulation by lipid and protein effectors, enabling rationale inhibitor design for this well-studied therapeutic target.

INTRODUCTION

The canonical mammalian phospholipase D (PLD) genes encode intracellular enzymes, which in response to extracellular signals generate the lipid second messenger phosphatidic acid (PA) via hydrolysis of phosphatidylcholine (PC), the most abundant phospholipid in cell membranes (Fig. 1a). PLD-generated PA regulates a multitude of cellular processes including activation of mTOR and MAPK pathways, vesicular trafficking and endocytosis, membrane fission and fusion, and cell growth, proliferation, and migration[1–3].

*To whom correspondence may be addressed. michael.airola@stonybrook.edu.

AUTHOR CONTRIBUTIONS

FZB performed all protein purifications, crystallization experiments, liposome sedimentation assays, docking experiments, and in vitro activity assays. CMS performed all cell based activity assays. JAB and TSH constructed key plasmids. FZB and MVA determined and refined the final crystal structure. FZB, MAF, and MVA contributed intellectual and strategic input. MAF and MVA supervised work. FZB, MAF, and MVA wrote and edited the final manuscript. All authors approved the final manuscript.

COMPETING FINANCIAL INTERESTS STATEMENT

The authors have no conflicting interest to report.

PLD has been identified as a therapeutic target for several diseases[4], including most prominently cancer[5,6], but also autoimmune[7,8], neurodegenerative[3,9], and cardiovascular disease[10]. Potent and specific small molecule inhibitors have been developed[11–13] and pharmacological inhibition is effective in preventing cancer cell invasion in cell culture[6], neoangiogenesis and metastasis[5], and thrombosis[14].

PLD is highly conserved in eukaryotes with two canonical isoforms (PLD1[15] and PLD2[16]) in humans. PLD1 and PLD2 are multi-domain proteins that include tandem PX/PH domains, a split-catalytic domain with dual HKD motifs presumed to self-dimerize into a single active site, and a C-terminal domain required for activity[17,18].

In contrast to PLD2, which is basally active, PLD1 activity is strongly stimulated by Protein Kinase C (PKC) and members of the Arf and Rho family of small GTPases, both *in vitro* and in cells[15,19]. The regulatory domain of PKC interacts directly with the N-terminal region of PLD1[18], whereas RhoA binds to PLD1's C-terminal region[20]. Phosphoinositides recruit PLDs to membranes through the tandem PX-PH domains[21], but phosphatidylinositol-(4,5)-bisphosphate (PIP_2) is also required as a co-factor for both basal PLD1 activity and stimulation by Arf, Rho, and PKC[19]. A polybasic motif adjacent to the second split-catalytic domain of PLD1 and PLD2 was proposed to function as the site that mediates PIP_2 binding and activation[21,22].

Despite thirty years of intensive biochemical and cell biology research into human PLD, the enzymes have remained structurally uncharacterized. Bacterial PLD isoforms have been crystallized, revealing the basic organization and action of the HKD motif during catalysis[23,24], but these enzymes are constitutively active and share limited homology with human PLDs. Thus, it has remained unclear how phosphoinositides and protein effectors stimulate PLD activity, and why the C-terminus is required for PLD activity. Here, we present the first crystal structure of recombinant human PLD1. The structure reveals the overall architecture of human PLDs, details of the catalytic cycle, and a novel phosphoinositide-binding polybasic pocket at the membrane interface. It also allows us to propose a mechanism for activation of PLD1 by RhoA.

RESULTS

Structure Determination.

In this study, we expressed in Sf9 cells a PLD1 protein construct ($Cat^{\Delta Ins}$) that lacks both the tandem PX-PH domains that regulate subcellular membrane association but are not required for enzymatic activity[18], and as well a PLD1-specific loop, predicted to be intrinsically disordered, that bridges the two catalytic HKD regions and is also not required for activity[18] (Fig. 1b). The crystal structure of this protein (human PLD1a residues 330–1074 Δ501–642), which contains ~60% of human PLD1, was determined to 1.8Å resolution (Supplementary Table 1). Experimental phases for the structure were obtained via single-wavelength anomalous diffraction by merging three datasets from a single crystal containing selenomethionine-enriched protein. PLD1 $Cat^{\Delta Ins}$ encompasses the two catalytic HKD motifs, the polybasic motif previously identified to be important for PIP_2 binding and activation, and the essential C-terminal domain (Fig. 1b). Attempts to crystallize the PLD1

catalytic domain (Cat^{WT}) with an intact loop were unsuccessful. The loop deletion sites between the two HKD domains were chosen by comparison with a subset of plant PLDs (*e.g. M. truncatula*) with no apparent loop (Supplementary Fig. 1a).

Prior to structure determination, the recombinant PLD1 $Cat^{\Delta Ins}$ protein used for crystallization experiments was verified to have activity only modestly reduced compared to the larger Cat^{WT} PLD1 protein containing the loop region (Fig. 1c), as well as an increased melting temperature that is indicative of a higher degree of stability (Supplementary Fig. 1b). The observed modest reduction in activity was comparable to a slightly different PLD1 $Cat^{\Delta Ins}$ protein (PLD1a residues 326–1074, Δ505–621) that exhibited a basal *in vitro* PLD activity that was 79% of that observed for full-length PLD1. PLD1 (326–1074, Δ505–621) activity was also stimulated by Rho and Arf small GTPases comparable to full-length PLD1[18], indicating that this mini-PLD1 protein is still subject to and capable of being regulated by its activators, and hence that its catalytic domain and the proposed RhoA-binding site are likely to be correctly folded[18].

Overall structure.

PLD1 $Cat^{\Delta Ins}$ contains 18 β-strands, 18 α-helices, and a series of ordered loops that combine to form a single asymmetric globular structure (Fig. 1d). All of the previously identified conserved regions in PLD1 are assembled into this single globular structure. Thus, we propose referring to the entire globular structure as the PLD1 “catalytic domain”, and specify residues 330–500 before the loop as HKD1, residues 643–967 after the loop as HKD2, and residues 968–1074, which exhibit no homology with bacterial PLD, as the C-terminal region (Fig. 1b, Supplementary Fig. 1a).

The asymmetric catalytic domain of PLD1 is built upon a symmetric core that is similar to bacterial PLD and composed of two 7-stranded mixed β-sheets flanked by α-helices. The two mixed β-sheets self-dimerize to form a single active site with the catalytic histidine and lysine residues of the two HKD motifs in close proximity (Fig. 1d, e, f). HKD1 creates 6 of the 7 β-strands in the first β-sheet with the last β-strand and α-helices completed by residues located after the loop in HKD2 (Fig. 1d). The second β-sheet is formed entirely by HKD2 and contains a cytoplasmic β-hairpin insertion (β16-β17, residues 936–949) between topological elements (Fig. 1d). The 142-amino acid loop that connects HKD1 and HKD2 and was excised for crystallization is located on the periphery of the structure (Fig. 1e).

Interspersed between the core topological elements of the two β-sheets are several unique structural elements that create the asymmetric structure and distinguish human PLD1 from other PLDs including bacterial PLD (Fig. 2). This includes elongated loops between the β2-β3 and β4-β5 strands in HKD1, residues between the last β6 strand in HKD1 and the first β7 strand in HKD2, an extended β11 strand in HKD2 that forms a β-hairpin with the β12 strand, a unique α10 helix in HKD2 above the core α11 helix, four α-helices and a single β-strand in the C-terminal region that pack against the β11-β12 hairpin and the α10 helix, and a C-terminal α18 helix near the active site (Fig. 1d).

The combined effects of these unique elements are two-fold. First, they create a 20Å deep, solvent-exposed cavity that starts at the membrane interface and leads directly down to the

active site (Fig. 3). The lower half of this cavity is 8Å deep, narrow (~8Å wide), and completely enclosed (Fig. 3a). This lower enclosed cavity contains the catalytic residues and other conserved polar residues that could mediate favorable hydrogen bond interactions with the glycerol backbone of phosphatidylcholine (Fig. 3b). Moving upwards towards the membrane interface, the cavity becomes increasingly more open in the shape of a funnel, enlarging to ~20Å wide at the top and enclosed on only two sides (Fig. 3a). The lower portions of the funnel are lined with hydrophobic residues that could interact with the non-polar hydrocarbon chains of the phosphatidylcholine substrate (Fig. 3b).

Second, these elements asymmetrically expand the surface area around and above the second core β-sheet of HKD2 (Fig. 1d). This expanded surface may interact with both the membrane during catalysis and the protein effectors that activate PLD1. In support of this, many of the previously identified mutations in PLD1 that disrupt activation by RhoA[25,26] cluster on this surface. The roles of these regions in activation by RhoA are discussed in more detail below.

The C-terminus.

Unlike the vast majority of proteins, the C-terminus of PLD1 is not solvent exposed but rather directed toward the interior of the protein, with the terminal carboxylic acid group of T1074 hydrogen bonding to the amide nitrogen atoms of both D916 and R917, which are adjacent to the active site (Fig. 1f). In addition, the last four C-terminal residues form a single-turn helix with the sidechains of V1072 and W1073 projecting into the lower hydrophobic part of the funnel that leads to the active site (Fig. 1f, 3b). Thus, T1074 functions as a keystone, folding back into the structure to stabilize key elements of the active site (Fig. 1d, f). These structural features are consistent with previous findings wherein deletion of the C-terminus inactivates PLD1, as well as the complete loss of activity upon fusion of PLD1 with a C-terminal epitope tag[17,18,27].

Active site and catalytic mechanism.

The catalytic mechanism of PLD enzymes is well characterized to proceed through a phosphohistidine intermediate that is formed after nucleophilic attack of the phospho-substrate by the first His residue of the HKD motif[23,24,28,29] (H464 in PLD1). The second His residue (H896 in PLD1) activates a water molecule that attacks the phosphohistidine to release product and regenerate the free catalytic His residue[29].

The two catalytic His residues of the HKD motifs in PLD1 are located 5Å apart at the interface of the two core β-sheets (Fig. 4). The N1 nitrogen atoms of both the H464 and H896 sidechains hydrogen bond to the acidic residues, E926 and D680 respectively, to increase their nucleophilic character (Fig. 4a). In support of the importance of these interactions, the point mutant E926Q in full-length PLD1 reduces PMA-stimulated PLD1 activity in cells by 75% (Fig. 4e).

Strong, positive electron density was observed in the Fo-Fc map off the N3 nitrogen of the H464 sidechain (Fig. 4d). This density was trigonal in shape. Similar density in bacterial PLD after an extended soak with phosphatidylcholine was modeled as a phosphohistidine[28]

(Fig. 4b). Thus, we modeled H464 as a phosphohistidine with a 1.8Å covalent bond between the N3 nitrogen and P phosphorous atoms (Fig. 4a).

The presence of this phosphohistidine allowed us to visualize specific interactions that may occur during catalysis. As previously proposed for other PLD members, both of the Lys residues of the HKD motif (K466 and K898) stabilize the oxygen atoms of the phosphohistidine (Fig. 4a). The Lys sidechains also form hydrogen bonds with the carbonyl oxygen atoms of the catalytic His residues and with the polar sidechains of D481, N913, and Q782. As expected, given their critical role, mutation of K466 and K898 results in a catalytically-dead version of PLD1[30]. Q782 also stabilizes the phosphohistidine oxygen atoms and was demonstrated to be important for full-length PLD1 activity (Fig. 4e), thereby replacing the function of a water molecule in bacterial PLD (Fig. 4b, c).

Above the phosphohistidine, a water molecule was observed in place for nucleophilic attack (Fig. 4a, d). As expected, H896 formed a hydrogen bond with this water molecule. Unexpectedly, a second residue, E828, also interacted with the water molecule. A salt bridge with R486 stabilized the position of E828. Both E828 and R486 were important in full-length PLD1, as E828A had a 50% reduction in activity and R486A had no detectable activity (Fig. 4e).

Taken together, this suggests PLD1 utilizes a ping-pong catalytic mechanism similar to that proposed for other PLD hydrolases with the Lys residues and additional active site residues stabilizing the phosphohistidine transition state.

Substrate recognition.

To gain insight into substrate recognition of the lipid PC by human PLD1, we used AutoDock Vina[31] to computationally predict the binding mode of PC. However, this failed to identify a consensus-binding mode for PC that was competent for catalysis (Fig. 3c). We therefore used a co-crystal structure of bacterial PLD covalently bound to short chain phosphatidic acid (6:0 PA) that was previously determined after a brief soak with the short chain substrate phosphatidylcholine (6:0 PC)[23]. Superposition of this co-crystal structure onto human PLD1 placed PA in the active site of PLD1 with the phosphate headgroup of PA next to the catalytic residue H464 (Fig. 3b). This allowed us to predict how PLD1 would recognize the glycerol backbone of PC using the product PA as a surrogate for PC. Residues W381, Y420, and R917, which are all directly above the catalytic HKD residues, were in position to putatively interact with the glycerol backbone of PC after minor rearrangements. Mutation of these residues eliminated or reduced full-length PLD1 activity in cells (Fig. 3d), which supports a role for W381, Y420, and R917 in catalysis and substrate recognition.

PIP_2 binding.

PLD1 requires PIP_2 as a co-factor for both basal activity and activation by RhoA, Arf, and PKC. As expected, PIP_2 strongly activated the catalytic domain of PLD1 by 73 fold, while $PI(3,4,5)P_3$ only mildly activated PLD1 by 5 fold (Supplemental Fig. 2a). Furthermore, PIP_2 and its headgroup IP3 increased the melting temperature of the PLD1 catalytic domain by 5 $^{\circ}C$ (Fig. 5a), and PIP_2 increased the association of PLD1 to liposomes (Supplemental Fig.

2b, Fig. 5b). This is consistent with previous reports that identified a PIP_2 binding "polybasic motif" in the catalytic domain of PLD2[22].

Surprisingly, the polybasic motif, previously identified as the PIP_2 binding and activation site, was distant from the membrane-binding interface and located on the bottom, cytoplasmic-facing surface of PLD1 (Fig 5c). To reassess where the PIP_2 interaction site might lie, we generated an electrostatic model of PLD1 that revealed five basic residues (K421, K435, R449, K708, K710) clustered together at the membrane interface (Fig. 5d). We refer to these residues as the "polybasic pocket", and the previously reported site as the "cytoplasmic polybasic motif" (Fig 5c).

Two of the polybasic pocket lysine residues are located at the end of the α4-helix facing the membrane surface. Found at the opposite end of this α4-helix are two of the amino acids previously identified as mediating PIP_2 binding (i.e., the cytoplasmic polybasic motif) (Supplemental Fig. 2c). We speculated that mutation of the cytoplasmic polybasic motif Arg residues (R691 and R695), which form extensive interactions at the base of the α4-helix (Fig. 5e), might potentially disturb the membrane facing-polybasic pocket at the top of the α4-helix. Thus, we hypothesized that the polybasic pocket, which is near the membrane interface, is the true PIP_2-binding and activation site in the PLD1 catalytic domain.

To test this hypothesis, we generated combined Ala point-mutants of residues in the polybasic pocket (K421A/K435A/R449A and K708A/K710A) in full-length PLD1. We also generated a double Ala point-mutant of the previously identified polybasic motif (R691A/R695A), which were originally mutated to Glycine[21]. All of these point mutants completely abolished PLD1 activity in cells (Fig. 5f).

To further confirm the role of the polybasic pocket in PIP_2 binding, we generated mutants in the context of $Cat^{\Delta Ins}$ and purified the proteins using insect cells. Liposome sedimentation analysis revealed the triple mutant K412A/K435A/R449A significantly reduced PIP_2-mediated liposome association, while the double polybasic pocket mutant K708A/K710A and polybasic motif mutant (R691A/R695A) had no affect (Supplemental Fig. 2d, Fig. 5g). Complete mutation of the polybasic pocket further reduced PIP_2-mediated liposome binding (Supplemental Fig. 2d, Fig. 5g). Taken together, this suggests that the membrane-facing polybasic pocket is indeed the likely PIP_2-binding and activation site and is essential for PKC-stimulated PLD1 activity.

PLD activation by Rho.

RhoA is one of the major protein effectors known to stimulate PLD1 *in vitro* and in cells[19,26]. Previous mutational analyses identified nine point-mutants that specifically disrupted RhoA activation[25,26]. Mapping the positions of these point mutants revealed that they all clustered on or around the α14 helix of the C-terminal region (Fig. 6a). These residues span the distance of the α14 helix, which is similar in size to RhoA. This allowed us to computationally predict the binding mode of GTP-loaded RhoA to PLD1 using Z-Dock[32] with the geranylgeranyl site of RhoA at the membrane interface and the switch I region of RhoA at the protein-protein interface with PLD1 (Fig. 6b). When RhoA activates PLD1, the K_M for PC is reduced[33]. Thus, it is tempting to speculate that RhoA binding to

the α14 helix of PLD1 induces conformational changes in PLD1 that propagate from the protein surface to the interior of the active site to increase substrate affinity.

DISCUSSION

Despite extensive effort, PLD1 has resisted structural characterization for decades. By focusing on the catalytic core of the enzyme and truncating the non-essential loop region, we provide here the first atomic-level view of human PLD1. This high-resolution structure reveals the overall architecture of PLD1, which harbors a 20Å deep active-site tunnel and several potential modes of regulation by PIP_2 and RhoA.

PLD1 is known to exhibit low basal activity in the absence of protein effectors and its lipid co-factor PIP_2[19]. Here, we confirm this biochemically with highly purified PLD1 protein. While PIP_2 is required for PLD1 activity (Supplemental Fig. 2a), the resulting rate of catalysis rate of 0.19 min^{-1} is extremely slow (Fig. 1c). This is not a result of deleting the loop region (Fig. 1c), or the lack of the tandem PX-PH domains, as the full-length protein and the catalytic region exhibit similar activity[18]. Rather, PLD1 also requires protein effectors that synergistically further stimulate activity more than 250-fold[19], bringing the turnover rate in-line with typical enzymes working on their preferred substrates.

Despite crystallizing PLD1 in the absence of protein effectors, we could not discern any clear and irrefutable structural reason for the low basal activity of PLD1. Our expectation, prior to visualizing the structure, was that we would observe occlusion of the active site by autoinhibition, similar to phospholipase C isozymes[34–36]. However, in our structure, the active site was unexpectedly solvent-exposed. We note that due to a lack of electron density, we could not model residues 829–833, which would sit above the active site. Thus, the possibility remains that PLD1 is autoinhibited by this dynamic section.

The presence of the phosphohistidine provides additional context. First, as it mimics the transition state of catalysis, it may induce conformational changes that reflect a partially-activated state of PLD1. The last residue we could accurately model above the active site, E828, has its sidechain directed into the active site and linked to the phosphohistidine by the nucleophilic water; thus it is plausible the phosphohistidine may be influencing the conformation of the adjacent residues. Alternately, the phosphohistidine itself may reflect the autoinhibited state of PLD1, as it represents a catalytically-inactive version incapable of forming the necessary covalent bond between H464 and PC to initiate hydrolysis. However, in the absence of supporting evidence, we are skeptical that the phosphohistidine plays an important role in PLD1 regulation *in vivo*.

While its functional role is unclear, the phosphohistidine did allow us to visualize interactions during the catalytic cycle. Most of these interactions were conserved with other PLDs, including bacterial PLD, thus establishing common themes for PLD-mediated catalysis. Several divergent residues were present in the active site of human PLD, with W381 and R917 most prominent (Fig. 3b). These residues have minor clashes with the superimposed PA molecule from bacterial PLD and likely contribute to substrate

recognition. However, the possibility exists that the position of these residues in the non-activated structure of PLD1 are autoinhibitory.

A major striking structural observation was the identification of a new PIP_2 activation polybasic pocket. The original PIP_2 polybasic motif was defined in the catalytic domain of human PLD2 based on biochemical evidence that mutation of the arginine residues to glycine eliminated PIP_2-mediated activation and liposome binding[22]. However, our structure revealed that these residues are on the cytoplasmic face of PLD1, which caused us to search for a more plausible PIP_2 activation site. In contrast, the new polybasic pocket (Fig. 1d,e, 6b) directly faces the membrane and thus is optimally positioned to participate in PIP_2 binding. Furthermore, our study revealed that this polybasic pocket is essential for PLD1 activity in cells, is important for association to PIP2-containing liposomes, and is consistent with the original polybasic region being impactful, as the two sites are structurally linked by the α4 helix.

With regards to protein effectors, our structure revealed that all of the previously identified mutations that disrupt RhoA activation map onto a single surface. RhoA activation could occur through two mechanisms: either by increasing productive association of PLD1 with membranes, or through inducing conformational changes in PLD1. Both appear likely: As the RhoA binding site is adjacent to the membrane interface, interaction with RhoA should increase the interfacial binding affinity of PLD1, and PLD1 activation is strongest when RhoA is geranylgeranylated[20]. In support of conformational changes, RhoA reduces the K_M of PLD1 for PC[33] and the RhoA binding site in PLD1 is structurally linked to the active site through a series of interactions. Thus, induction of minor conformational changes at the peripheral RhoA-binding site could readily propagate to the active site.

Arf1 and PKC are the two additional PLD1 activators. PKC targets the N-terminus of PLD1[18], thus our structure provides no insight into this process. Arf1 directly activates the catalytic domain but binds to it only weakly at best, and there are no known mutations that disrupt Arf1 activation. Arf1 and RhoA synergistically activate PLD1[19,37], so distinct sites of interaction on the catalytic domain are anticipated, but we cannot currently speculate on the nature of the Arf1-stimulatory site.

ONLINE METHODS

Plasmid constructs.

Residues 330–1074 of human PLD1a (Cat^{WT}), i.e. an N-terminally truncated protein lacking the tandem PX-PH domains, was cloned into pFastBac Htb (Gibco, Life Technologies) with a TEV-cleavable N-terminal 6xHis-Tag using SfoI and NotI restriction sites. Overlap extension was used to remove the loop in PLD1 to create "$Cat^{\Delta Ins}$" (human PLD1a residues 330–1074 Δ501–642). *In vivo* expression analyses were conducted using the full-length coding region of PLD1 cloned into pCGN, which appends an N-terminal HA-tag[15]. Mutations in pFastBac-PLD-$Cat^{\Delta Ins}$ and pCGN-HA-PLD1 were introduced using overlap extension. All constructs were verified by direct sequencing.

Protein expression and purification.

PLD1 Cat^{WT}, PLD1 Cat$^{\Delta Ins}$, and PLD1 Cat$^{\Delta Ins}$ mutants were expressed in Sf9 cells using baculovirus. 800 mL of cells were infected with 4 mL of baculovirus at 2–4 million cells/mL at >95% viability and harvested 48 hours later. Cell pellets were lysed in 50 mM Tris, pH 7.5, 400 mM NaCl, 5 mM Imidazole, 5% glycerol and the lysates centrifuged at 22,000 rpm and passed through a 0.22 μm filter. PLD1 protein was purified with a 5 mL HisTrap FastFlow column (GE Healthcare) followed by size exclusion chromatography using a HiLoad 26/600 Superdex 200 pg column in 20 mM Tris, pH 7.0, 150 mM NaCl. PLD1 ΔINS and WT PLD1 were concentrated to 2.79 and 0.91 mg/mL, respectively, flash-frozen, and stored at −80°C.

Selenomethionine-enriched PLD1 Cat$^{\Delta Ins}$ protein was expressed following the protocol described by Cronin et al.[38], using SFM-900 media (Invitrogen) with exchange to SFM-900 Methionine(−) Cysteine(−) media (Invitrogen) doped with selenomethionine 16 hours after baculoviral infection. Selenomethionine-enriched PLD1 Cat$^{\Delta Ins}$ protein was purified using the batch method. The filtered lysate was incubated with 2 mL nickel NTA agarose beads (Goldbio) for one hour and then applied to a column, washed with 30 mM imidazole buffer, eluted with 300 mM imidazole buffer, and finally applied to a Superdex 200 column.

Crystallization, data collection, structure determination, and refinement.

Purified PLD1 Cat^{WT} protein was screened for crystallization using JCSG sparse matrix screens, but none of the ~400 conditions yielded promising crystal hits. We hypothesize that this was specifically because of inclusion of the intrinsically disordered and quite large loop region, as such regions have a high degree of entropy and are known to prevent ordered crystal packing. PLD1 Cat$^{\Delta Ins}$ crystal conditions were identified using JCSG sparse matrix screens by mixing a 1:1 ratio of protein to mother liquor. Four PEG 3350 citrate salt conditions produced rod-like crystals. Micro-seeding using a seed-bead (Hampton Research) and solution optimization generated single rod-like crystals using hanging-drop vapor diffusion in 0.2 M ammonium citrate, pH 5.3, 12% PEG 3350 at RT. Native diffraction data was collected at the Brookhaven National Laboratory FMX beamline and scaled using DIALS XDS in CCP4[39].

Selenomethionine PLD1 Cat$^{\Delta Ins}$ formed crystals under similar conditions as the native protein. Three complete 360-degree SAD datasets were collected at 12660.37 eV in 15-degree wedges from a large, single, rod-like crystal at the APS GM/CA 23ID-B beamline and processed using in-house APS processing software[40]. Since the anomalous signal was weak for each individual dataset, the three unmerged mtz files were scaled and merged using the Phenix “Scale and Merge” program[41]. Strong anomalous signal to 4.5 Å was detected with Xtriage. 9/12 methionine sites were detected using the Hyss program[42]. Phasing of the data was carried out with Autosol[43] and an initial model generated using Autobuild[44] with an initial Rwork/Rfree of 0.373/0.4209. After manual model building in coot[45] and several refinements in Phenix Refine[46], the generated model was used for molecular replacement with the higher 1.8Å resolution native data set. Additional model building in Coot and refinement in Phenix produced the final model (Table 1) (PDB code: 6U8Z).

In vitro PLD1 activity assay.

PLD1 activity was measured by tracking the release of ^{3}H-choline from radiolabeled phosphatidylcholine (American Radiolabeled Chemicals, Inc.) using Triton X-100 mixed micelles. The final concentration and ratios of the mixed-micelles contained 1 mM Triton X-100 and the lipids 117 μM dioleoylphosphatidylcholine (DOPC, Avanti Polar Lipids) and 58 μM Brain PI(4,5)P_2 (Avanti Polar Lipids) (ratio = 85:10:5 mol%) that were doped with ^{3}H-labeled POPC. The DOPC and PI(4,5)P_2 lipids were mixed and dried under a gentle stream of nitrogen gas, resuspended in reaction buffer containing 1 mM Triton X-100, 100 mM HEPES, pH 7.5, 160 mM KCl, 3 mM EGTA and sonicated until the solution was clear. 25 μL of purified human PLD1 protein and 25 μL of mixed-micelles were mixed and incubated at 37°C for 30 minutes and then quenched with a 2:1 chloroform:methanol solution. After vortexing and centrifugation, the aqueous layer, which contained the ^{3}H-choline released product, was extracted and CPMs quantitated using a scintillation counter. All reactions were linear with respect to enzyme concentration and time. Total radioactivity per 25 μL was measured; blanks were determined using buffer in place of enzyme.

Cellular PLD1 activity assay.

Enzymatic activity was measured based on PLD1's ability to catalyze a transphosphatidylation reaction using 1-butanol to generate phosphatidylbutanol[47,48]. HEK293T cells were incubated overnight in a 6-well plate and transfected in full media the next day with PLD1 expression plasmids using Fugene (Promega). 12–16 hours post-transfection, cells were labeled with [^{3}H]-palmitate (ART 129; American Radiolabeled Chemicals) and cultured for 24 hours. The radiolabeled media was then replaced with Opti-MEM and the cells cultured for 1–2 hours prior to the addition of 0.3% butanol and 100 nM PMA. After 30 minutes, cold methanol was added to stop the reaction and the lipids were extracted and dried using a speed vacuum and resuspended in chloroform/methanol (19:1) containing 50 μg of non-radiolabeled phosphatidylbutanol (Avanti Polar Lipids) to enable location of the labeled enzymatic product on TLC plates (Whatman LK5DF). The plates were then developed as previously described[47,48] and the lipids visualized using iodine flakes (Sigma-Aldrich) and scraped into 5 mL of scintillation fluid for quantification.

Liposome binding assay.

1 mM liposomes were generated with DOPC (Avanti Polar Lipids) and Brain PI(4,5)P_2 (Avanti Polar Lipids) in 20 mM Tris, pH 7.5, 150 mM NaCl, mixed with 10 μM PLD1 $Cat^{\Delta Ins}$ or PLD1 $Cat^{\Delta Ins}$ mutants, and then incubated at RT for 30 minutes. The liposome-protein mixture was pelleted at 100,000 × g for one hour. The soluble fraction was removed, the pellet resuspended in an equal volume, and both samples resolved on SDS-PAGE.

Thermal shift assay.

PLD1 $Cat^{\Delta Ins}$ and PLD1 Cat^{WT} were diluted in 20 mM Tris, pH 7.5, 150 mM NaCl to 0.4 mg/mL with 8x Sypro Orange (Sigma Aldrich). SYPRO orange fluorescence was measured on an RT-PCR instrument with a temperature increase of 1 degree Celsius/min. Fluorescence was normalized to the highest measured value and then fit to a non-linear Boltzmann sigmoidal curve. Melting temperature was determined from the associated temperature of

50% normalized fluorescence. Protein was mixed with either 0.5 mM d-myo-1,4,5-triphosphate (Cayman) or 0.5 mM PtdIns-(4,5)-D2(1,2-dihexanoyl) (Cayman). Melting temperatures were compared with protein in buffer alone.

AutoDock Vina.

Phosphatidylcholine was docked into the PLD1 structure using Autodock Vina 1.1.2[31] . Autodock Tools[49] was used to generate the phosphatidylcholine molecule, generate the area for docking, and select the flexible residues of PLD1. 9 states for the phosphatidylcholine docking were generated and the model was selected based on orientation of the phosphatidylcholine as to direct the head group towards the catalytic core.

Z-Dock.

The PLD1-RhoA complex was computationally predicted using Z-DOCK 3.0.2[32]. PLD1 model (6U8Z) and RhoA-GTP model (1A2B) were selected as input proteins. Residues on α14 of PLD1, which are required for interaction with RhoA and subsequent PLD1 activation, were selected as binding site residues. The selected model was determined through examination of the top 10 generated complexes, prioritizing proper membrane-facing orientation of the RhoA C-terminus.

Data availability.

Coordinates and structure factors have been deposited in the Protein Data Bank under accession code 6U8Z. All other data are available from the authors on request.

Supplementary Material

Refer to Web version on PubMed Central for supplementary material.

ACKNOWLEDGMENTS

We thank the staff at the FMX and GM/CA-CAT beamlines for assistance during data collection. Beamline FMX (17-ID-2) is operated by LSBR, supported by NIH/NIGMS (P41GM111244) and DOE/BER (KP1605010. GM/CA@APS has been funded in whole or in part with Federal funds from the NCI (ACB-12002) and the NIGMS (AGM-12006). The Eiger 16M detector was funded by an NIH-Office of Research Infrastructure Programs, High-End Instrumentation Grant (S10 OD012289). This research used resources of the APS, a U.S. Department of Energy (DOE) Office of Science User Facilities operated for the DOE Office of Science by Argonne National Laboratory (under Contract No. DE-AC02-06CH11357). This work was also supported by the NIH awards: R35GM128666 (MVA), T32GM092714 (FZB), and R01GM084251 (MAF), the NSF award: 1612689 (CMS), a Carol Baldwin Breast Cancer Award (MAF), and a Chhabra-URECA award (JAB).

REFERENCES

1. Bruntz RC, Lindsley CW & Brown HA Phospholipase D signaling pathways and phosphatidic acid as therapeutic targets in cancer. Pharmacol Rev 66, 1033–79 (2014). [PubMed: 25244928]
2. Jenkins GM & Frohman MA Phospholipase D: a lipid centric review. Cell Mol Life Sci 62, 2305–16 (2005). [PubMed: 16143829]
3. Tanguy E, Wang Q & Vitale N Role of Phospholipase D-Derived Phosphatidic Acid in Regulated Exocytosis and Neurological Disease. Handbook of experimental pharmacology (2018).
4. Frohman MA The phospholipase D superfamily as therapeutic targets. Trends Pharmacol Sci 36, 137–44 (2015). [PubMed: 25661257]

5. Chen Q et al. Key Roles for the Lipid Signaling Enzyme Phospholipase D1 in the Tumor Microenvironment During Tumor Angiogenesis and Metastasis. Science Signaling 5, ra79–ra79 (2012). [PubMed: 23131846]
6. Scott SA et al. Design of isoform-selective phospholipase D inhibitors that modulate cancer cell invasiveness. Nature chemical biology 5, 108–117 (2009). [PubMed: 19136975]
7. Göbel K et al. Phospholipase D1 mediates lymphocyte adhesion and migration in experimental autoimmune encephalomyelitis. European Journal of Immunology 44, 2295–2305 (2014). [PubMed: 24811005]
8. Kang DW et al. Phospholipase D1 Has a Pivotal Role in Interleukin-1-Driven Chronic Autoimmune Arthritis through Regulation of NF-B, Hypoxia-Inducible Factor 1, and FoxO3a. Molecular and Cellular Biology 33, 2760–2772 (2013). [PubMed: 23689131]
9. Lindsley CW & Brown HA Phospholipase D as a therapeutic target in brain disorders. Neuropsychopharmacology 37, 301–2 (2012). [PubMed: 22157867]
10. Elvers M et al. Impaired IIb 3 Integrin Activation and Shear-Dependent Thrombus Formation in Mice Lacking Phospholipase D1. Science Signaling 3, ra1–ra1 (2010). [PubMed: 20051593]
11. Brown HA, Thomas PG & Lindsley CW Targeting phospholipase D in cancer, infection and neurodegenerative disorders. Nature Reviews Drug Discovery 16, 351–367 (2017). [PubMed: 28209987]
12. Monovich L et al. Optimization of halopemide for phospholipase D2 inhibition. Bioorg Med Chem Lett 17, 2310–1 (2007). [PubMed: 17317170]
13. Su W et al. 5-Fluoro-2-indolyl des-chlorohalopemide (FIPI), a Phospholipase D Pharmacological Inhibitor That Alters Cell Spreading and Inhibits Chemotaxis. Molecular Pharmacology 75, 437–446 (2009). [PubMed: 19064628]
14. Stegner D et al. Pharmacological Inhibition of Phospholipase D Protects Mice From Occlusive Thrombus Formation and Ischemic Stroke-Brief Report. Arteriosclerosis Thrombosis and Vascular Biology 33, 2212–2217 (2013).
15. Hammond SM et al. Human ADP-ribosylation factor-activated phosphatidylcholine-specific phospholipase D defines a new and highly conserved gene family. J Biol Chem 270, 29640–3 (1995). [PubMed: 8530346]
16. Colley WC et al. Phospholipase D2, a distinct phospholipase D isoform with novel regulatory properties that provokes cytoskeletal reorganization. Current Biology 7, 191–201 (1997). [PubMed: 9395408]
17. Liu MY, Gutowski S & Sternweis PC The C Terminus of Mammalian Phospholipase D Is Required for Catalytic Activity. Journal of Biological Chemistry 276, 5556–5562 (2001). [PubMed: 11083860]
18. Sung TC, Zhang Y, Morris AJ & Frohman MA Structural analysis of human phospholipase D1. Journal of Biological Chemistry 274, 3659–3666 (1999). [PubMed: 9920915]
19. Hammond SM et al. Characterization of Two Alternately Spliced Forms of Phospholipase D1. The Journal of Biological Chemistry 272, 3860–3868 (1997). [PubMed: 9013646]
20. Yamazaki M et al. Interaction of the small G protein RhoA with the C terminus of human phospholipase D1. J Biol Chem 274, 6035–8 (1999). [PubMed: 10037681]
21. Du G et al. Regulation of phospholipase D1 subcellular cycling through coordination of multiple membrane association motifs. J Cell Biol 162, 305–15 (2003). [PubMed: 12876278]
22. Sciorra VA et al. Identification of a phosphoinositide binding motif that mediates activation of mammalian and yeast phospholipase D isoenzymes. Embo Journal 18, 5911–5921 (1999). [PubMed: 10545103]
23. Leiros I, McSweeney S & Hough E The Reaction Mechanism of Phospholipase D from Streptomyces sp. Strain PMF. Snapshots along the Reaction Pathway Reveal a Pentacoordinate Reaction Intermediate and an Unexpected Final Product. Journal of Molecular Biology 339, 805–820 (2004). [PubMed: 15165852]
24. Leiros I, Secundo F, Zambonelli C, Servi S & Hough E The first crystal structure of a phospholipase D. Structure 8, 655–67 (2000). [PubMed: 10873862]
25. Cai S & Exton JH Determination of interaction sites of phospholipase D1 for RhoA. Biochem J 355, 779–85 (2001). [PubMed: 11311142]

26. Du G et al. Dual requirement for rho and protein kinase C in direct activation of phospholipase D1 through G protein-coupled receptor signaling. Mol Biol Cell 11, 4359–68 (2000). [PubMed: 11102529]
27. Zhang Y, Altshuller YM, Hammond SM, Morris AJ & Frohman MA Loss of receptor regulation by a phospholipase D1 mutant unresponsive to protein kinase C. EMBO J. 18, 6339–6348 (1999). [PubMed: 10562546]
28. Gottlin EB, Rudolph AE, Zhao Y, Matthews HR & Dixon JE Catalytic mechanism of the phospholipase D superfamily proceeds via a covalent phosphohistidine intermediate. Proc Natl Acad Sci U S A 95, 9202–9207 (1998). [PubMed: 9689058]
29. Stuckey JA & Dixon JE Crystal structure of a phospholipase D family member. Nat Struct Biol 6, 278–84 (1999). [PubMed: 10074947]
30. Sung TC. , R. R, Zhang Y, Rudge SA, Temel R, Hammond SM, Morris AJ, Moss B, Engebrecht J, Frohman MA. Mutagenesis of phospholipase D defines a superfamily including a trans-Golgi viral protein required for poxvirus pathogenicity. EMBO J. 16, 4519–4530 (1997). [PubMed: 9303296]
31. Trott O & Olson AJ AutoDock Vina: Improving the speed and accuracy of docking with a new scoring function, efficient optimization, and multithreading. Journal of Computational Chemistry, 31(2), 455–461 (2010). [PubMed: 19499576]
32. Pierce BG et al. ZDOCK server: interactive docking prediction of protein-protein complexes and symmetric multimers. Bioinformatics 30, 1771–1773 (2014). [PubMed: 24532726]
33. Henage LG, Exton JH & Brown HA Kinetic Analysis of a Mammalian Phospholipase D. Journal of Biological Chemistry 281, 3408–3417 (2006). [PubMed: 16339153]
34. Hicks SN et al. General and versatile autoinhibition of PLC isozymes. Molecular cell 31, 383–394 (2008). [PubMed: 18691970]
35. Lyon AM et al. An autoinhibitory helix in the C-terminal region of phospholipase C-β mediates Gαq activation. Nature structural & molecular biology 18, 999–1005 (2011).
36. Lyon AM, Begley JA, Manett TD & Tesmer JJ Molecular Mechanisms of Phospholipase C β3 Autoinhibition. Structure 22, 1844–1854 (2014). [PubMed: 25435326]
37. Henage LG Kinetic Analysis of a Mammalian Phospholipase D. Journal of Biological Chemistry 281, 3408–3417 (2006). [PubMed: 16339153]
38. Cronin Ciarán N., L. KB, Rogers Joe. Production of selenomethionyl-derivatized proteins in baculovirus-infected insect cells. Protein Science 16, 2023–2029 (2007). [PubMed: 17660253]
39. Waterman DG et al. Diffraction-geometry refinement in theDIALSframework. Acta Cryst. 72, 558–575 (2016).
40. Pothineni SB et al. Tightly integrated single- and multi-crystal data collection strategy calculation and parallelized data processing in JBluIce beamline control system. 47, 1992–1999 (2014).
41. Terwilliger TC et al. Can I solve my structure by SAD phasing? Planning an experiment, scaling data and evaluating the useful anomalous correlation and anomalous signal. Acta Crystallographica Section D Structural Biology 72, 359–374 (2016). [PubMed: 26960123]
42. Grosse-Kunstleve RW & Adams PD Substructure search procedures for macromolecular structures. Acta Crystallographica Section D Biological Crystallography 59, 1966–1973 (2003). [PubMed: 14573951]
43. Terwilliger TC et al. Decision-making in structure solution using Bayesian estimates of map quality: the PHENIX AutoSol wizard. 65, 582–601 (2009).
44. Terwilliger TC et al. Iterative model building, structure refinement and density modification with thePHENIX AutoBuildwizard. Acta Crystallographica Section D Biological Crystallography 64, 61–69 (2008). [PubMed: 18094468]
45. Emsley P, Lohkamp B, Scott WG & Cowtan K Features and development ofCoot. Acta Crystallographica Section D Biological Crystallography 66, 486–501 (2010). [PubMed: 20383002]
46. Afonine PV et al. Towards automated crystallographic structure refinement withphenix.refine. Acta Crystallographica Section D Biological Crystallography 68, 352–367 (2012). [PubMed: 22505256]
47. Morris AJ, Frohman MA & Engebrecht J Measurement of phospholipase D activity. Anal Biochem 252, 1–9 (1997). [PubMed: 9324933]

48. Philip F, Ha EE, Seeliger MA & Frohman MA Measuring Phospholipase D Enzymatic Activity Through Biochemical and Imaging Methods. Methods Enzymol 583, 309–325 (2017). [PubMed: 28063496]

49. Morris GM et al. AutoDock4 and AutoDockTools4: Automated docking with selective receptor flexibility. Journal of Computational Chemistry 30, 2785–2791 (2009). [PubMed: 19399780]

50. Ali I et al. Structure of the tandem PX-PH domains of Bem3 from Saccharomyces cerevisiae. Acta Crystallographica Section F Structural Biology Communications 74, 315–321 (2018). [PubMed: 29718000]

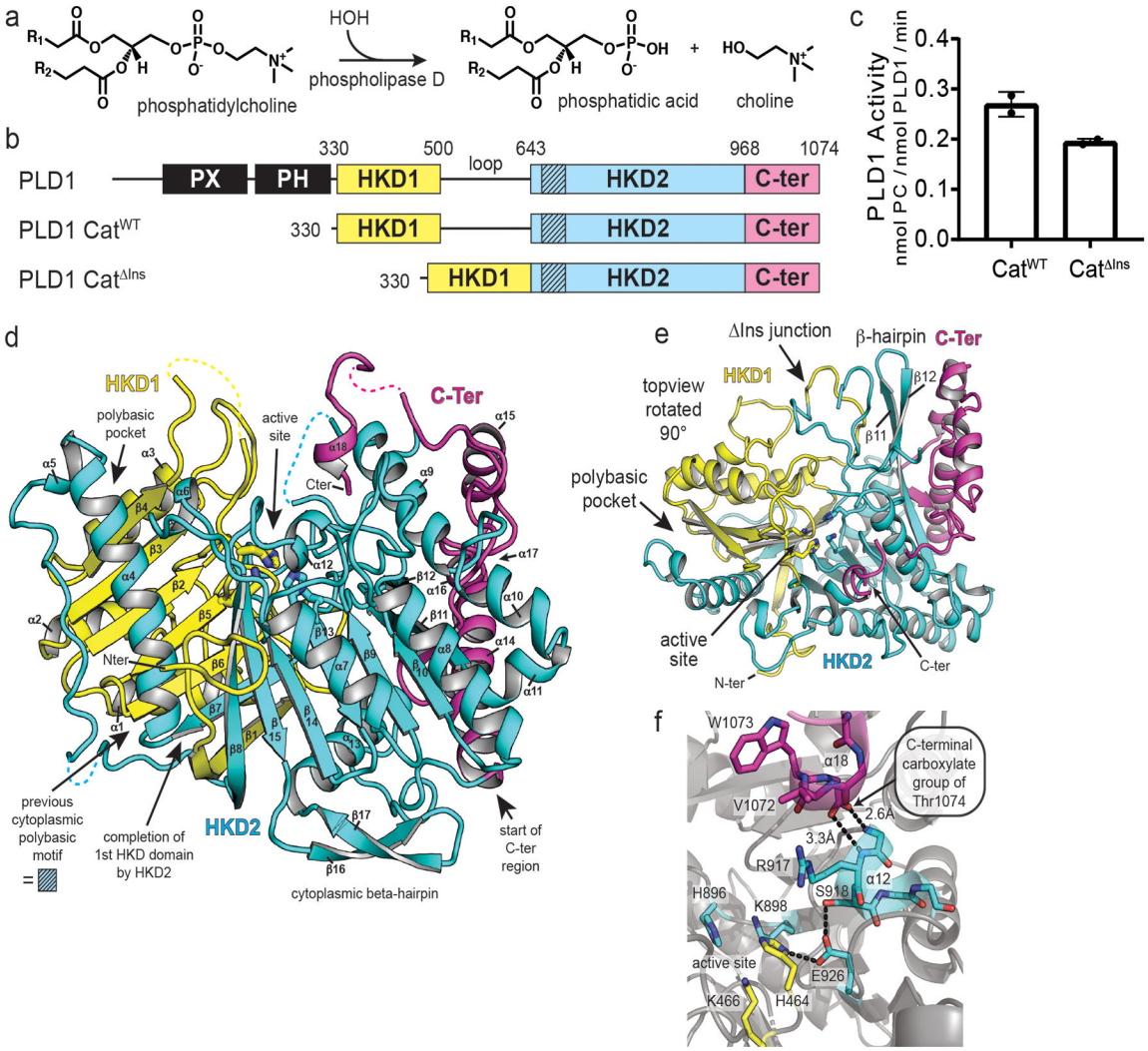

Figure 1. Structure of human PLD1.

(a) Phosphatidylcholine hydrolysis by PLD produces phosphatidic acid and choline. **(b)** Diagram of PLD1 domains drawn to scale, with black tandem PX-PH domains, yellow HKD1, cyan HKD2, and magenta C-terminal domain. The shaded box denotes the previous polybasic motif PIP_2 site. **(c)** *In vitro* assay of the purified PLD1 catalytic domain with (Cat^{WT}) and without ($Cat^{\Delta Ins}$) the loop region. Data are the means and SDs of two experiments performed in triplicate. **(d)** Overall structure of the PLD1 catalytic domain. **(e)** View of PLD1 looking down from the membrane interface. **(f)** Close up view of the C-terminal carboxylic acid group hydrogen bonding to the α12 helix to help form and stabilize the active site.

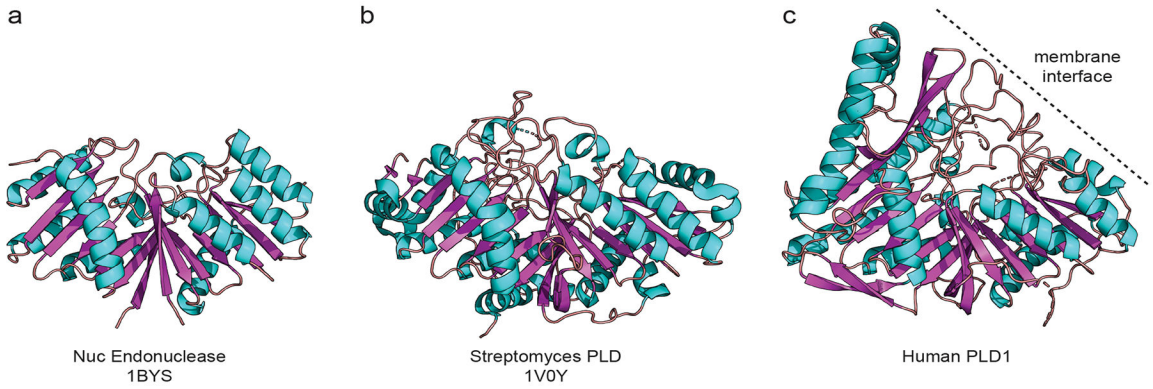

Figure 2. Structural comparison of PLD family phosphodiesterases with human PLD1.

These enzymes all feature topologically similar β-sheet cores, flanked by α-helices, that dimerize with the catalytic His and Lys residues of the HKD motifs at the dimer interface. **(a)** Symmetric structure of Nuc-endonuclease from two identical subunits that dimerize (PDB entry 1BYS). **(b)** Near symmetric structure of *Streptomyces* PLD from a single polypeptide chain that self-dimerizes (PDB entry 1V0Y). **(c)** In comparison, human PLD1 exhibits an asymmetric structure from topological insertions that form a tunnel to the active site and expand the surface area for membrane binding and protein interactions.

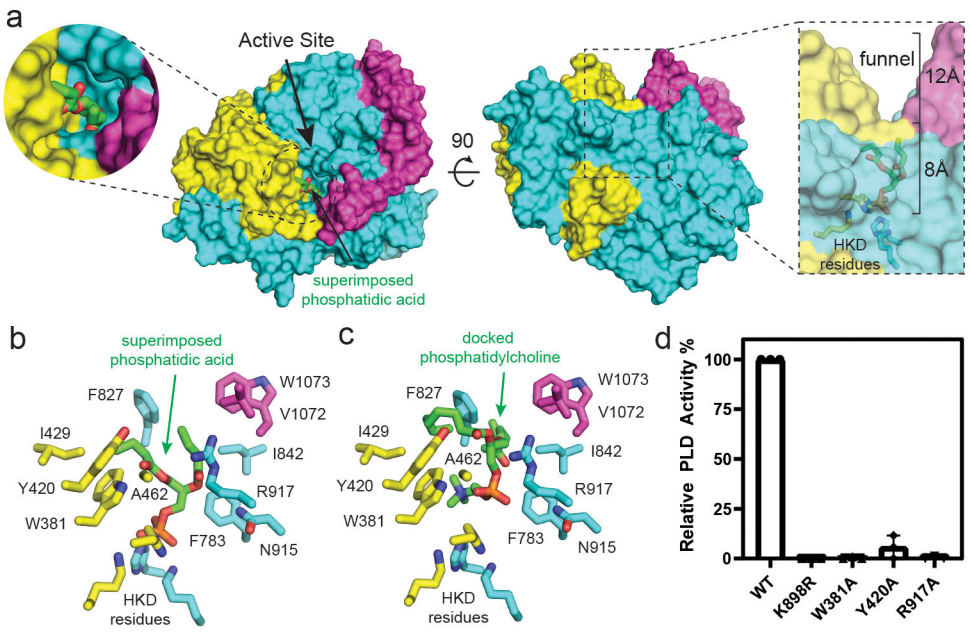

Figure 3. Active site cavity in PLD1.

(a) Surface representation of human PLD1 looking down into the active site cavity formed by topological insertions in HKD1 (yellow), HKD2 (cyan), and the C-terminal region (magenta). PA (green sticks) from a Streptomyces PLD co-crystal structure is superimposed in the active site. Inset displays a transparent side surface view with the short chain PA completely buried within the enclosed 8Å deep lower cavity. The upper 12Å funnel section would accommodate the extended acyl chains of membrane-bound phospholipids. **(b)** View of active site residues in close proximity to the superimposed PA that could form favorable interactions with the polar glycerol backbone and non-polar aliphatic acyl chains of the substrate PC. **(c)** View of active site residues in close proximity to PC docked with AutoDock Vina. **(d)** Cellular activity assay of PLD1 substrate recognition mutants. Activity normalized to WT PLD1 at 100% and catalytically-dead PLD1 K898R at 0%. Data are the means and SDs of three experiments performed in duplicate.

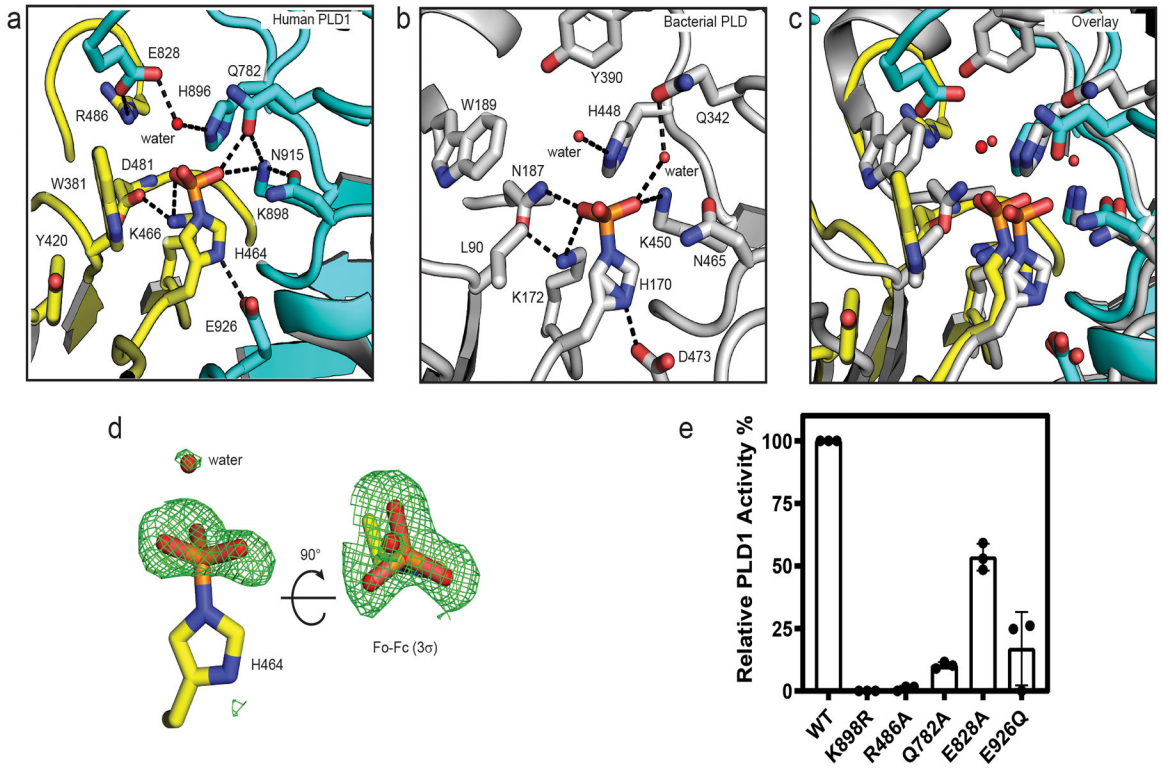

Figure 4. A phosphohistidine intermediate helps define the catalytic cycle of PLD1.

(a) Active site of human PLD1. Dashed lines denote hydrogen bond or salt bridge interactions. HKD1 residues indicated in yellow, HKD2 residues indicated in cyan. **(b)** Active site of *Streptomyces* PLD (PDB entry 1V0V) with similar phosphohistidine as in panel **b**. **(c)** Overlay of human PLD1 and *Streptomyces* PLD active sites. **(d)** Positive Fo-Fc electron density map, shown in green mesh and contoured at 3σ, prior to modeling His464 as a phosphohistidine. Phosphohistidine is shown as sticks with yellow carbon, blue nitrogen, red oxygen, and orange phosphorous. The water molecule inline for nucleophilic attack is shown as a red sphere. **(e)** Cellular activity assay of PLD1 active-site mutants. Activity normalized to WT PLD1 at 100% and catalytically-dead PLD1 K898R at 0%. Data are the means and SDs of three experiments performed in duplicate.

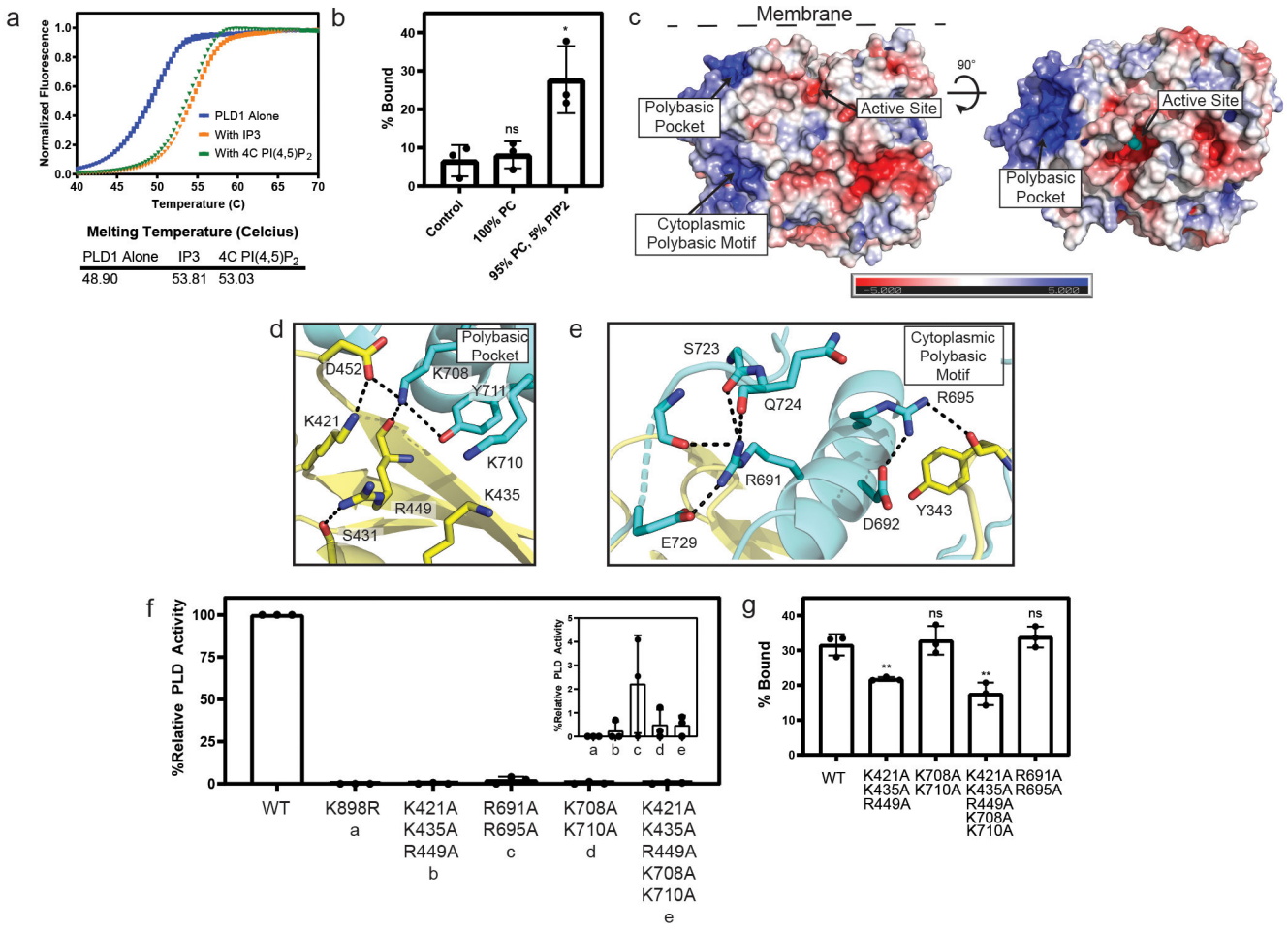

Figure 5. A polybasic pocket defines a new PIP_2 activation site at the membrane.

(**a**) PIP_2 and IP3, the PIP_2 headgroup, increase the melting temperature of PLD1 by differential scanning fluorimetry. **(b)** Quantification of liposome association of PLD1. Data are the means and SDs of three experiments. Asterisk (*) indicates a P value < 0.05. **(c)** Electrostatic surface representations of PLD1 identify a polybasic pocket at the membrane interface. Sideview (left) and topview looking down from the membrane (right). Red indicates acidic surfaces, blue basic surfaces, white neutral surfaces. **(d)** Structural interactions of the polybasic pocket. Black dotted lines indicate polar interactions. (**e**) Stick representations of the cytoplasmic polybasic motif, previously proposed as the PIP_2 activation site **(f)** Cellular activity of PLD1 PIP_2-mutants. Activity normalized to WT PLD1 at 100% and catalytically-dead PLD1 K898R at 0%. Data are the means and SDs of three experiments performed in duplicate. **(g)** Quantification of liposome association of wild-type (WT) PLD1 $Cat^{\Delta Ins}$ and mutants. Data are mean and SDs of three experiments. Double asterisks (**) indicate a P value < 0.005.

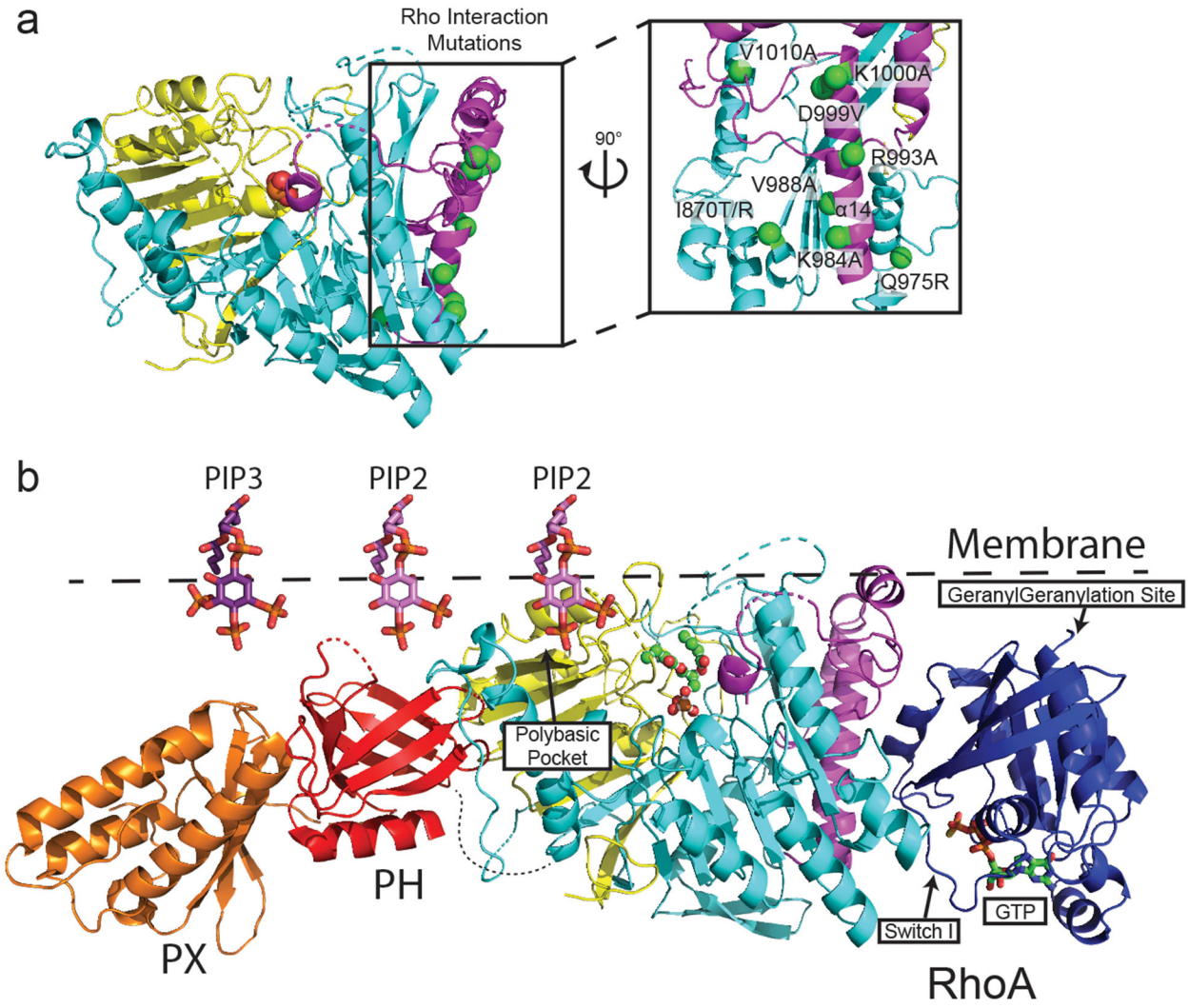

Figure 6. Model of RhoA activation of PLD1.

(a) Distribution of point mutations that disrupt RhoA interaction and/or activation of PLD1 on the 3D structure. All mutations cluster around a single surface between the C-terminal region (magenta) and HKD2 (cyan). Cα atoms of mutations are shown as green spheres. **(b)** Model created with Z-dock of interfacial catalysis by full-length PLD1 bound to docked GTP-loaded RhoA (dark blue) with the RhoA geranylgeranyl site at membrane interface. Key membrane lipid interactions in PLD1 are denoted. Tandem PX-PH domains modeled from the *S. cerevisiae* Bem3 structure[50] (PDB entry 6FSF).